Reduction of laser power threshold for melting tungsten due to subsurface helium holes

Cite as: J. Appl. Phys. **100**, 103304 (2006); https://doi.org/10.1063/1.2387151
Submitted: 19 April 2006 . Accepted: 08 September 2006 . Published Online: 22 November 2006

Shin Kajita, Dai Nishijima, Noriyasu Ohno, and Shuichi Takamura

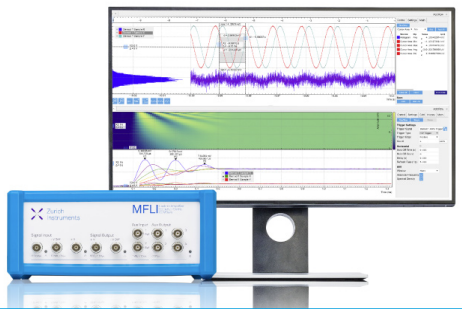

Reduction of laser power threshold for melting tungsten due to subsurface helium holes

Shin Kajita[a] and Dai Nishijima[b]
Graduate School of Engineering, Nagoya University, Nagoya 464-8603, Japan

Noriyasu Ohno
EcoTopia Science Institute, Nagoya University, Nagoya 464-8603, Japan

Shuichi Takamura
Graduate School of Engineering, Nagoya University, Nagoya 464-8603, Japan

(Received 19 April 2006; accepted 8 September 2006; published online 22 November 2006)

Interactions between nanosecond laser pulses and a tungsten substrate having submicron holes near the surface formed by exposure to helium plasmas are investigated experimentally and numerically. After tungsten surface having helium holes was irradiated by nanosecond laser pulses in helium plasmas, scanning electron microscope micrographs of the tungsten surface show that the roughness of the surface is significantly enhanced under certain experimental conditions. For an understanding of the physical mechanisms to arise the phenomena, heat conduction in the substrate having holes is modeled by solving a three-dimensional heat conduction equation. The model calculations show that the surface reaches a melting point locally even if the pulse energy is low enough to lead to the melting of a virgin substrate. On the basis of surface temperature calculations and from an evaluation of the tensile stress put on the lid of the hole, repetitive explosions of the helium holes caused by heating the lids are considered to be the mechanism enhancing the surface roughness. Simultaneous irradiation of laser pulses and the helium ions may have a drilling effect on tungsten with repetitive formation and explosions of the subsurface helium holes. © *2006 American Institute of Physics*. [DOI: 10.1063/1.2387151]

I. INTRODUCTION

Tungsten, which has high thermal properties and a low sputtering yield, has been widely used where high heat fluxes are concentrated. It is also frequently used for electrostatic probe tips used to measure electron density and temperature in plasmas. Moreover, tungsten is a candidate for a divertor material in magnetic confinement fusion devices and a candidate material for the first wall of inertial fusion reactors, DEMO, and future commercial fusion reactors.[1] However, recent experimental observations reveal that bubbles and holes are formed on the tungsten surface when it is exposed to helium plasmas even when the incident ion energy is less than the threshold energy for physical sputtering.[2–4] The formation of holes and bubbles may lead to the degradation of tungsten's superior properties, and this could cause problems in some cases.

Transient heat flux accompanied by disruptions and edge localized modes[5] (ELMs) provides a high heat load to a target material during a short time period in the operation of a tokamak. In type-I ELMs of the International Thermonuclear Experimental Reactor (ITER), a heat flux of above several MJ m^{-2} is expected during 0.1–1 ms;[6] moreover, in the disruption of ITER, a heat load of several tens of MJ m^{-2} is expected during a time period of the order of 10 ms. For inertial fusion reactor design, the heat load to the first wall is considered to be ~500 J m^{-2} during 1 ns due to x rays and ~10 kJ m^{-2} during several microseconds due to burn ions.[7] Thus, there is a concern that the transient heat load on a tungsten surface having bubbles and holes may pose serious problems and possibly melt the tungsten, which would result in an increase of high Z material in core plasmas and have material losses.

Further, a problem has been reported in the measurement of negative ion density using a laser photodetachment method,[8,9] in which an electrostatic probe surface is exposed to nanosecond laser pulses. When helium gas is contained in plasmas, the formation of bubbles on the probe tip surface may lead to an increase of the probe current, and consequently, the negative ion density should be seriously overestimated.[8] Because the laser pulse energy was sufficiently lower than the threshold energy for tungsten ablation, it is thought that laser pulse irradiations to tungsten with holes and bubbles lead to the physical phenomena that are different from that occurring when laser pulses are irradiated to virgin tungsten.[9,10]

To investigate physical phenomena caused by transient heat load to a tungsten substrate having holes and bubbles, we performed nanosecond laser irradiation experiments while the substrate was exposed to plasmas. Experimental observations reveal that the roughness of the surface is significantly enhanced due to transient heat load under certain experimental conditions even though the laser pulse energy is low enough to lead to melting or vaporization of virgin tungsten.

On the basis of our experimental observations, we devel-

[a]Electronic mail: kajita@ees.nagoya-u.ac.jp
[b]Present address: National Institute of Advanced Industrial Science and Technology, Saga 841-0052, Japan.

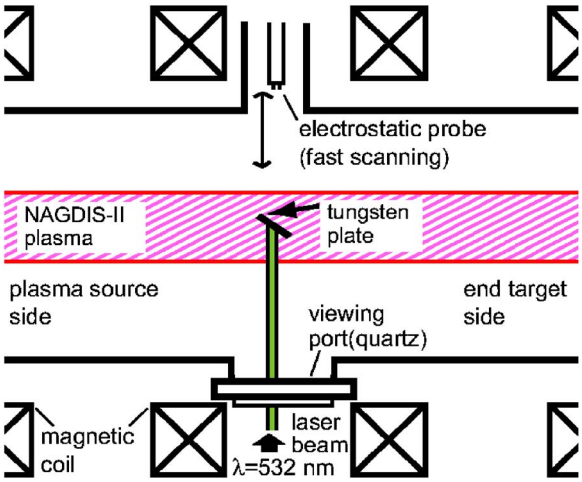

FIG. 1. (Color online) Experimental setup for laser irradiation experiments to tungsten surface.

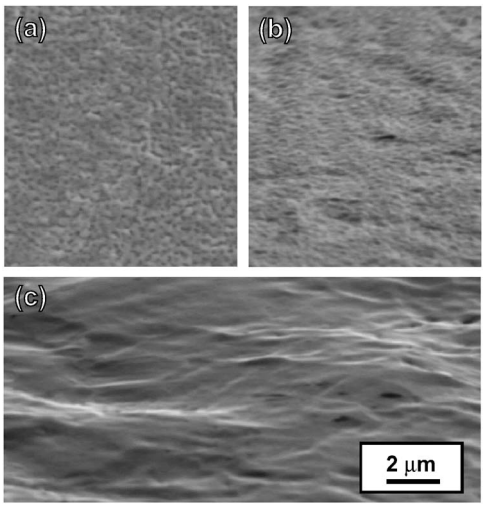

FIG. 2. (a) and (b) are the SEM images of tungsten exposed to helium plasma at a surface temperature of 1200 K during 7200 s from both top and oblique directions, respectively. (c) shows a SEM image of the surface from an oblique direction after laser pulse irradiation at 360 mJ cm^{-2}.

oped a three-dimensional heat transfer model, which includes the effect of holes, to analyze heat conduction in a solid substrate and liquid melt. Although the actual configuration is more complicated than the simple modeled configuration, our model including holes should constitute a benchmark for temperature changes in response to laser pulses. With the results of the calculations of surface temperature and the evaluations of the tensile stress put on the lids of holes, we discuss the physical phenomena occurring during the interactions between the transient heat load and the tungsten substrate with holes. The experimental setup and the experimental results are shown in Sec. II. In Sec. III, after the calculation model is presented, the physical mechanisms causing the enhancement of the surface roughness are discussed based on those calculations. The paper is concluded in Sec. IV.

II. EXPERIMENTS

A. Experimental setup

Experiments were performed in a linear divertor plasma simulator NAGDIS-II (Nagoya divertor simulator II). Detailed descriptions of the device have been reported in Refs. 11 and 12. Plasmas were generated by dc arc discharge between a LaB_6 cathode and anode. A magnetic field of 0.1 T suppressed the diffusion of the plasmas across the magnetic field, and a cylindrical plasma of ~2 m in length was formed. Typical electron density and temperature in helium plasmas are $\sim 10^{19}$ m^{-3} and ~5 eV, respectively. Ion flux was measured with an electrostatic probe.

Figure 1 shows a schematic view of the experimental setup. Tungsten sample was situated at about a 45° angle to the magnetic field line. The sample was powder metallurgy tungsten of 0.2 mm in thickness. The second harmonic of a Nd:YAG laser (yttrium aluminum garnet) (Continuum, SLII-10), wavelength of 532 nm, was used as the photon source. Pulse duration Δt_{pulse} was 5–7 ns, and the pulse interval was 0.1 s, which is long enough for the surface to recover to the initial surface temperature. The laser beam had a 2 mm diameter, sufficiently greater than the characteristic length of heat conduction (<1 μm) during the pulse duration of 5–7 ns. The laser beam was injected through a quartz viewing port at an angle of 90° to the magnetic field line. Laser pulse energy was measured outside the vacuum chamber, and the input energy per unit area at the target was deduced by considering the transmission rate at the viewing port and the angle of the laser beam to the tungsten sample. The temperature of the sample was measured with a radiation pyrometer.

B. Experimental results

Scanning electron microscope (SEM) images of the tungsten sample exposed to helium plasmas at the surface temperature of 1200 K are shown in Figs. 2(a) and 2(b). Figures 2(a) and 2(b) are micrographs taken from the top and oblique directions, respectively.

In this experiment, the ion flux and incident ion energy were 4.5×10^{22} m^{-2} s^{-1} and 24 eV, respectively, and the sample was exposed to helium plasmas over a period of 7200 s. A roughness of several hundreds of nanometers in size is observed on the surface. Although, from the previous NAGDIS-II study, bubbles of ~5 nm in size were observed by transmission electron microscopy (TEM) analysis at a temperature of 1300 K,[4] it is difficult to observe bubbles and holes by SEM in this temperature range. It is worthwhile to note that in this case the surface color changed to black after being exposed to helium plasma. This black colored surface cannot be seen in the experiments at the higher surface temperature shown later.

Figure 2(c) shows SEM micrographs of a sample after being irradiated by the laser pulses in the helium plasma. The sample was exposed to the helium plasma over a period of 3600 s, and then the laser pulses irradiated the sample during a further 3600 s exposure to the helium plasma. The laser pulse energy was 3.6 kJ m^{-2} (360 mJ cm^{-2}) per pulse. In Fig. 2(c), the surface roughness disappeared; it became smooth. Visual observation shows that the black colored surface seemed to recover to a surface having a metallic luster after

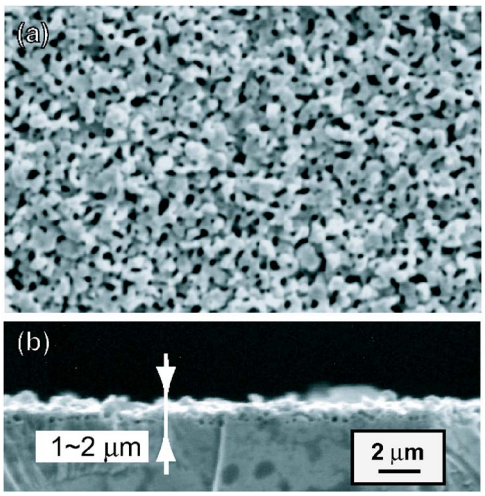

FIG. 3. (Color online) SEM images of tungsten exposed to helium plasmas at a surface temperature of 1700 K during 3600 s: (a) surface and (b) cross section.

irradiated by the laser pulses. It is speculated that the surface reached its melting point due to the laser pulses, and consequently, the rough structures on the surface were mitigated.

Figures 3(a) (from top) and 3(b) (cross section) show the SEM images of the tungsten sample exposed to helium plasmas under different experimental conditions. In this experiment, the ion flux and the incident ion energy were, respectively, 1.7×10^{23} m^{-2} s^{-1} and 27 eV, and the surface temperature was ~1700 K. The tungsten was exposed to the helium plasmas over a period of 3600 s. Many black spots can be observed where pinholes appear on the surface. Furthermore, Fig. 3(b) shows that the holes are observed not only on the surface but also in the subsurface region. The size of the holes was several hundreds of nanometers, and the depth penetration of the holes was 1–2 μm under the experimental conditions. For investigating the mechanisms of the formation of the helium bubbles and holes, detailed experiments have been performed in NAGDIS-II;[3,4] two necessary conditions to promote the formation of holes with high helium ion flux have been suggested.[4] One condition relates to the incident helium ion energy ($\geqslant$5 eV) and the other to the substrate temperature ($\geqslant$1500 K). The experimental conditions where the incident energy of the helium ions was 27 eV and the surface temperature was ~1700 K corresponded to the ones indicated as promoting the formation of helium holes.

Pinholes and subsurface bubbles have also been observed during annealing of helium implanted materials.[13] Although these phenomena could not be understood using conventional bubble migration and coalescence theory, the results using computer simulation suggest that the phenomena can be attributed to the breakaway bubbles swelling during the bubble growth process.[14] It is likely that the pinholes observed in Fig. 3(a) were formed by similar physical mechanisms to the ones in the cases of annealing. Thus, it seems that superlarge bubbles grow to bisect the surface, and consequently pinholes are observed in Fig. 3.

Figures 4(a) and 4(b) are SEM micrographs of laser irradiated tungsten in helium plasma at a bulk temperature of

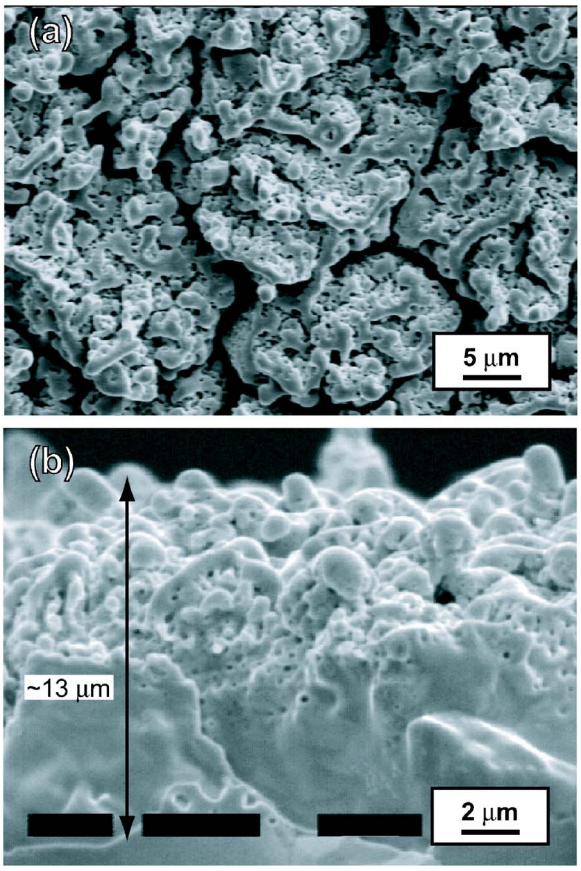

FIG. 4. (Color online) (a) and (b) are SEM images of tungsten irradiated by laser pulses during exposure to helium plasmas: (a) surface (×2000) and (b) cross section (×5000). The bulk temperature of the sample, ion flux, and incident ion energy were 1700 K, 1.7×10^{23} m^{-2} s^{-1}, and 27 eV, respectively. The laser pulse energy was 200 mJ cm^{-2}.

~1700 K taken from the top (surface) and side (cross section), respectively. After the sample was exposed to helium plasmas for a period of 1800 s under the same condition as in Fig. 3, the sample was then irradiated by the laser pulses for a period of 1800 s while it was also exposed to the helium plasma. The laser pulse energy was 2 kJ m^{-2} (200 mJ cm^{-2}) per pulse, and 18 000 pulses were irradiated. The sizes of the holes were much larger than those without laser irradiation. Furthermore, we can observe cracks on the surface, which may have been caused by the rapid temperature change in response to the laser irradiation. The cross section shown in Fig. 4(b) represents that the penetrating depth of the holes became ~10 μm, which was significantly greater than that without laser irradiations shown in Fig. 3(b).

We also performed laser irradiation experiments in a deuterium plasma and in vacuum using the same sample with helium holes as shown in Fig. 3. Figures 5(a) and 5(b) show cross sections of the laser irradiated sample in vacuum and in deuterium plasma, respectively. In deuterium plasma, the ion flux and incident ion energy were 3.5×10^{21} m^{-2} s^{-1}, and 20 eV, respectively. The bulk sample temperatures during the irradiation of the sample were in (a) room temperature and in (b) 800 K. The laser pulse energies were both ~4 kJ m^{-2} (400 mJ cm^{-2}) per pulse, which was two times greater energy than that of Fig. 4, and 18 000 pulses were

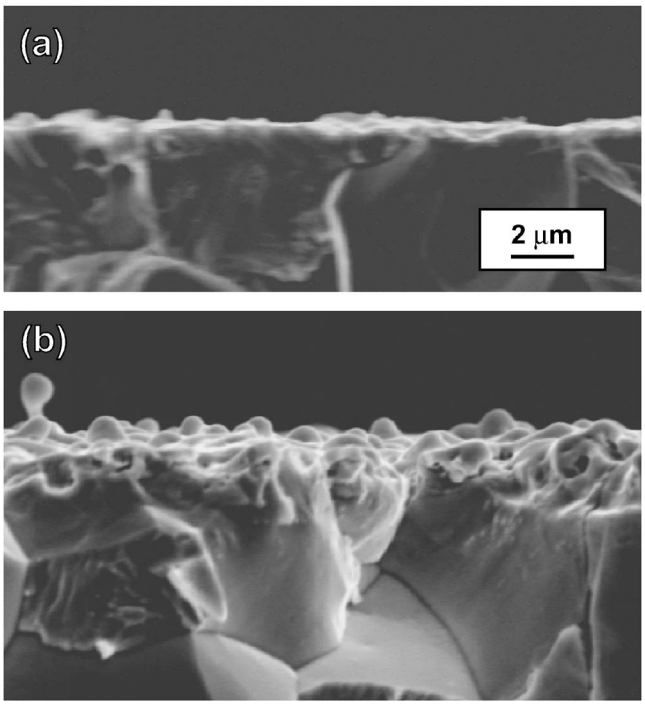

FIG. 5. (a) and (b) show the cross section of a laser irradiated sample that had helium subsurface holes in vacuum and in deuterium plasma, respectively. The laser pulse energy was 400 mJ cm^{-2}.

irradiated to the sample. Because the laser pulse energy was greater than that of Fig. 4, the surface may have reached the melting point in these cases. Particularly, in the case of Fig. 5(b), we can observe melting traces on the surface. However, contrary to the simultaneous irradiation of helium plasma and laser pulses shown in Fig. 4, the surface roughness became moderate after being irradiated by the laser pulses in deuterium plasmas and in vacuum, although the sample had subsurface holes before the laser pulse irradiations. These results indicate that surface roughness is not enhanced so much without high helium ion flux, even if a surface having helium holes is irradiated by laser pulses.

However, because many factors including the bulk temperature of the substrate, surface nature, ion flux to the sample, species of ion, and laser pulse energy can change the phenomena, further experimental investigations are necessary. Although it is difficult to determine the necessary conditions to significantly enhance the roughness of the surface, the phenomenon itself is the specific characteristic of the interaction between a transient heat flux and a surface having subsurface holes. Thus, it is important to discuss the physical processes accompanying the phenomenon. For virgin tungsten, we can analytically estimate the surface temperature change in response to the laser pulse. It has been found that it is difficult to reach the melting point when the surface condition is virgin tungsten, even if the initial substrate temperature is 1700 K.[10] We estimated that decreasing thermal diffusivity by 50% may lead to surface melting.[15] However, when the penetrating length of the surface modification, l_{mod}, is sufficiently shorter than the characteristic length of the heat transfer during the laser pulse duration, l_{heat}, the complete phenomenon cannot be explained by the concept of the degradation of thermal diffusivity. Particularly, phenomena caused by the nonuniformity of the temperature due to the fine structures in the substrate, such as the holes, cannot be taken into consideration. Under the experimental conditions, $l_{\mathrm{mod}} \sim 1-2\ \mu\mathrm{m}$ and $l_{\mathrm{heat}} \sim \sqrt{\kappa t_{\mathrm{pulse}}} < 1\ \mu\mathrm{m}$, so that nonuniformity of temperature due to the fine structures can occur. Therefore, we developed a three-dimensional calculation model to analyze the effect of holes on temperature change. In the next section, we discuss the physical mechanisms of the phenomenon in response to laser pulse irradiation to a surface having helium holes based on the calculation results. An evaluation using the model calculations may provide us with a physical microscopic picture.

III. TEMPERATURE ANALYSIS OF THE SURFACE WITH SUBSURFACE HOLES

A. Calculation model

For investigating the physical mechanism to change the feature of the substrate as shown in Figs. 4(a) and 4(b), we analyzed the temporal evolution of the substrate temperature in response to transient heat load. Temporal evolution of the surface temperature can be evaluated by solving the following heat conduction equation:

$$\frac{1}{\kappa}\frac{\partial T}{\partial t} = \frac{\partial^2 T}{\partial x^2} + \frac{\partial^2 T}{\partial y^2} + \frac{\partial^2 T}{\partial z^2} + \frac{Q(z,t)}{K}, \tag{1}$$

where T is the surface temperature in Kelvins, x and y are distances along the two directions parallel to the surface, z is distance from the surface, κ is the thermal diffusivity in $m^2\ s^{-1}$, and K is the thermal conductivity in $W\ m^{-1}\ K^{-1}$.

In Eq. (1), $Q(z,t)$ is the energy intensity absorbed by the metal in $W\ m^{-3}$ and can be written as

$$Q(z,t) = (1-R_s)I(t)\frac{\exp(-z/l_p)}{l_p}, \tag{2}$$

where $I(t)$ is the laser fluence in $W\ m^{-2}$, R_s is the surface reflectivity, and l_p is the absorption penetration depth written as

$$l_p = \sqrt{\frac{2}{\mu\sigma_M\omega}}. \tag{3}$$

Here, μ is magnetic permeability, σ_M is electric conductivity,[16,17] and ω is angular frequency. Because σ_M is a function of temperature, l_p also depends on temperature. For laser pulses with a wavelength of 532 nm, l_p is ~10 nm at 1000 K and ~20 nm at 3000 K. In usual cases, the skin effect is negligible because the penetration depth is sufficiently shorter than the characteristic length of heat conduction during laser pulse duration. However, the effect is included for the sake of considering the effects of holes, because in some cases lid thickness is comparable to the penetration depth. The deposited energy in the lid is written as

$$(1-R_s)I(t)[1-\exp(-t_{\mathrm{lid}}/l_p)]. \tag{4}$$

Table I shows the absorption rate of the energy in the lid at various temperatures and lid thicknesses assuming that R_s

TABLE I. Absorption rate of energy in the lid calculated from Eq. (4) at different temperatures and lid thicknesses.

Temperature (K)	Thickness (nm)		
	10	30	50
1000	0.61	0.94	0.99
2000	0.47	0.85	0.96
3000	0.39	0.77	0.91

=0. Absorption rate decreases as temperature increases and lid thickness decreases. The absorption rate is larger than 0.9 if the lid thickness is greater than 50 nm. If the lid thickness becomes thinner, the transmitted laser heats are transferred into the inner side of the hole. However, this effect is not taken into account in the present model. Though the effect may increase the temperature at the bottom of the hole when t_{lid} is smaller than a few tens of nanometers, it is thought that the transmitted power does not change the surface temperature significantly.

Additionally, the effect of radiation from the surface is neglected, because radiation power calculated from the Stefan-Boltzmann law $\sigma_{\mathrm{SB}}T_{\mathrm{surface}}^4$,[18] where σ_{SB} and T_{surface} are the Stefan-Boltzmann constant and surface temperature, respectively, is significantly smaller than the heat flux due to the laser pulses. Specifically, even if the surface temperature is at the melting point of 3700 K, the radiation from the surface is $\sim$10 MW m^{-2}, while the heat flux due to the laser pulses is $>$100 GW m^{-2}. As for thermal conductivity, the data in Ref. 16 were used below the melting point, and K =70.5 W m^{-1} K^{-1} was used above the melting point. As for thermal diffusivity κ, which is written as $\kappa=K/c_p\rho$ using specific heat capacity c_p and density ρ, the value was evaluated using the data of c_p in Ref. 19 with ρ of 19 000 kg m^{-3}.

It is reported that the cohesive energy is reduced if the ratio of the surface atoms to the inside atoms is fairly large because the surface atoms are less stable than the inside atoms.[20] Consequently, the melting temperature may decrease. Under the calculated conditions, however, the effect is neglected because it is not so important. Based on the theory in Ref. 20, the number of the bond energy of a surface atom is about $\sim$1/4 of that of an inside atom. Even if the lid thickness is 10 nm, which is the minimum lid thickness used in the present paper, about 35 atomic layers exist in the lid. Thus, the reduction degree of cohesive energy is estimated to be $\sim$4% for the lid thickness of 10 nm. Further, it is noted that the melting temperature may reduce if the nanosized bubbles exist in the lid layer. However, in the present model, the regions are separated to two distinct regions, namely, bulk tungsten and hole, so that the effect is not included and remained as a future work.

Equation (1) was discretized using an alternating direction implicit (ADI) method.[21] The temperature at the time step $n+1$, T_{n+1}, is obtained from the value at n, T_n, after three steps of partial discretization. We used the following scheme of second-order accuracy, which may also be considered as a stabilizing correction scheme as proposed by Jim Douglas.[22]

$$\frac{T_n^* - T_n}{\kappa\Delta t} = \frac{\Delta_x^2}{2}(T_n^* + T_n) + \Delta_y^2 T_n + \Delta_z^2 T_n, \tag{5}$$

$$\frac{T_n^{**} - T_n}{\kappa\Delta t} = \frac{\Delta_x^2}{2}(T_n^* + T_n) + \frac{\Delta_y^2}{2}(T_n^{**} + T_n) + \Delta_z^2 T_n, \tag{6}$$

$$\frac{T_{n+1} - T_n}{\kappa\Delta t} = \frac{\Delta_x^2}{2}(T_n^* + T_n) + \frac{\Delta_y^2}{2}(T_n^{**} + T_n) + \frac{\Delta_z^2}{2}(T_{n+1} + T_n). \tag{7}$$

Here, $\Delta_x^2 T$, $\Delta_y^2 T$, and $\Delta_z^2 T$ represent $[T(i+1,j,k)-2T(i,j,k)+T(i-1,j,k)]/\Delta x^2$, $[T(i,j+1,k)-2T(i,j,k)+T(i,j-1,k)]/\Delta y^2$, and $[T(i,j,k+1)-2T(i,j,k)+T(i,j,k-1)]/\Delta z^2$, respectively, where i, j, and k are the step numbers along the x, y, and z directions, respectively, and Δx, Δy, and Δz, respectively, correspond to the step lengths along each direction. Equations (5)–(7) can be simplified by subtracting Eq. (5) from Eq. (7) and Eq. (6) from Eq. (7), respectively. The resulting equations become

$$\left(\Delta_x^2 - \frac{2}{\kappa\Delta t}\right)T_n^* = -\left(\Delta_x^2 + 2\Delta_y^2 + 2\Delta_z^2 + \frac{2}{\kappa\Delta t}\right)T_n, \tag{8}$$

$$\left(\Delta_y^2 - \frac{2}{\kappa\Delta t}\right)T_n^{**} = \Delta_y^2 T_n - \frac{2}{\kappa\Delta t}T_n^*, \tag{9}$$

$$\left(\Delta_z^2 - \frac{2}{\kappa\Delta t}\right)T_{n+1} = \Delta_z^2 T_n - \frac{2}{\kappa\Delta t}T_n^{**}. \tag{10}$$

When the temperature reaches the melting point T_m of 3700 K, the enthalpy function is used to account for the phase change considering the latent heat of fusion.[23] The enthalpies under and over T_m are, respectively,

$$h(T) = \int_0^T \rho(T)c_p(T)dT \quad (T < T_m), \tag{11}$$

$$h(T) = \int_0^T \rho(T)c_p(T)dT + L_m \quad (T > T_m), \tag{12}$$

where L_m is the latent heat of fusion, 4.8×10^9 J m^{-3} (46 kJ mol^{-1}).[16] The maximum and minimum enthalpies at T_m are

$$h_{\mathrm{min}} = \int_0^{T_m} \rho(T)c_p(T)dT, \tag{13}$$

$$h_{\mathrm{max}} = \int_0^{T_m} \rho(T)c_p(T)dT + L_m, \tag{14}$$

respectively. The temperature does not increase during $h_{\mathrm{min}} < h < h_{\mathrm{max}}$.

Figure 6 shows a schematic illustration of the model for numerical calculations. To introduce the effect of holes, four holes of the same size are located at the four corners in the calculation region. The radius of a hole and its depth at the center are indicated as R_h and L_h, respectively.

For the boundary conditions at the boundaries in the x

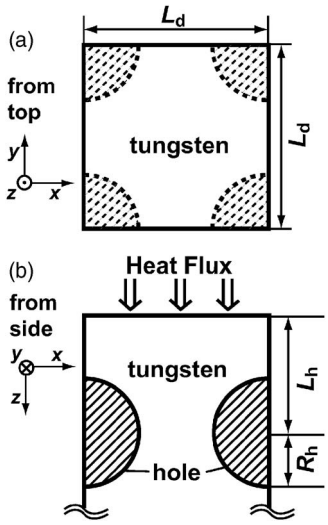

FIG. 6. Illustration of our calculation model: (a) from the top and (b) from the side.

and y directions, the gradient of the temperature is fixed to *zero*, namely,

$$\left.\frac{\partial T}{\partial x}\right|_{\text{edge}(x)} = \left.\frac{\partial T}{\partial y}\right|_{\text{edge}(y)} = 0. \tag{15}$$

On the other hand, at the boundary in the z direction, the temperature is fixed to be the bulk temperature of the substrate as

$$T_{\text{edge}(z)} = T_{\text{bulk}}. \tag{16}$$

This boundary condition is reasonable if $\Delta z \times$(grid number) is sufficiently deeper than the characteristic length of heat conduction during the relevant time period. At the boundary between a hole and the substrate, the gradient of the temperature is also set to zero such that the heat is not conducted toward the hole. This assumption is applicable under the present conditions, because the heat capacity of the helium in the hole, $c_p\rho$, is $\sim$15 kJ m^{-3} K^{-1} at 10 MPa,[24] which is sufficiently lower than that for tungsten of $\sim$300 kJ m^{-3} K^{-1}. If the hole radius is smaller than several tens of nanometers, the value of $c_p\rho$ in the hole becomes comparable to that of tungsten because the pressure in the hole increases with the decrease of the hole's radius as shown later, so that a more precise investigation might be necessary. Initially, the entire temperature is at the bulk temperature,

$$T(x,y,z,t=0) = T_{\text{bulk}}. \tag{17}$$

In the present paper, the grid sizes were $\Delta x = \Delta y = \Delta z = 10$ nm, and the time step size Δt was 10^{-12} s, which is short enough to sustain the stability of the calculations for the grid size. Grid meshes consisting of $100 \times 100 \times 200$ of uniformly spaced nodes were used. In the present paper, surface reflectivity is assumed to be zero, because the surface reflectivity of tungsten decreases as increasing the ion fluence,[25] and may become close to zero if the ion fluence is over 10^{26} m^{-2}.[26] It is reported that surface reflectivity changes as a function of laser intensity when the ultrashort pulse is irradiated to solid targets.[27,28] However, the laser intensity in the present study is of the order of 10^7–10^8 W/cm^2, which is significantly lower than the typical intensity used in the subpicosecond laser physics (10^{13}–10^{18} W/cm^2), so that the effect is negligible under the present conditions. To compare the calculation results with the experimental observations, the bulk temperature and the laser power were chosen to be the same values as the experimental ones, i.e., 1700 K and 200 mJ cm^{-2}, respectively. The temporal evolution of the laser pulse was simplified to be a triangular shape with a rising and falling time of 3.5 ns. This assumption well approximated the Gaussian time dependence.[29]

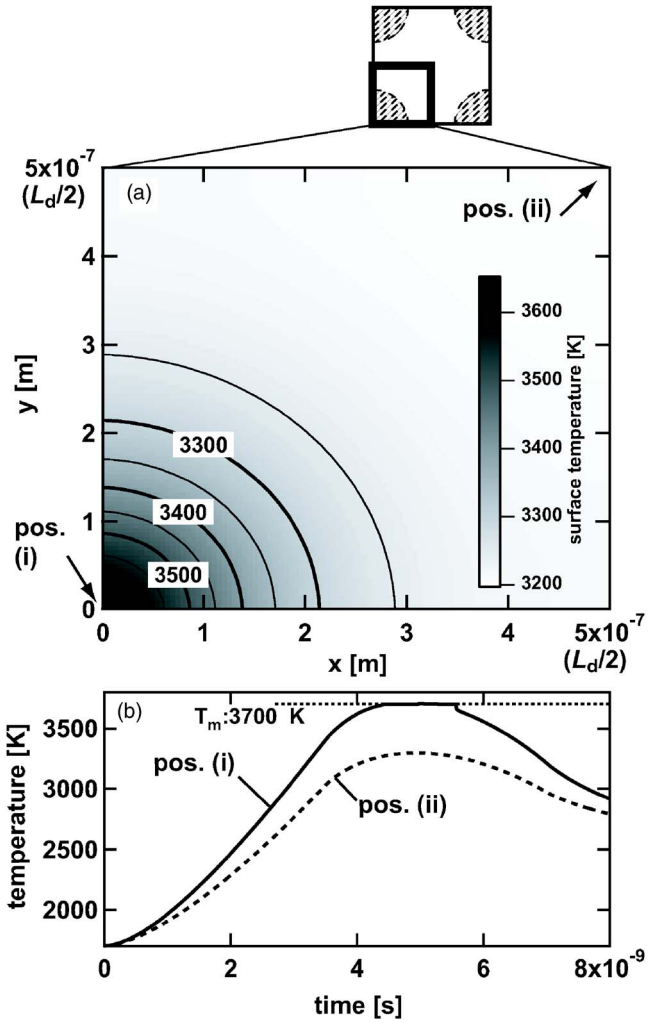

FIG. 7. (Color online) (a) Calculated surface temperature profile at 4.5 ns. Laser power was 200 mJ cm^{-2}, and the shape of the laser pulse was a triangular temporal evolution having rising and falling times of 3.5 ns. (b) Temporal evolutions of the surface temperature at positions (i) and (ii). (R_h = 150 nm, L_h = 200 nm.)

B. Results and discussion

Figure 7(a) shows the surface temperature profile in a fourth part of the calculated region at 4.5 ns. In this calculation, L_h and R_h were 200 and 150 nm, respectively. We can see that the surface temperature is not uniform but that the temperature above the hole [lower left in Fig. 7(a), position

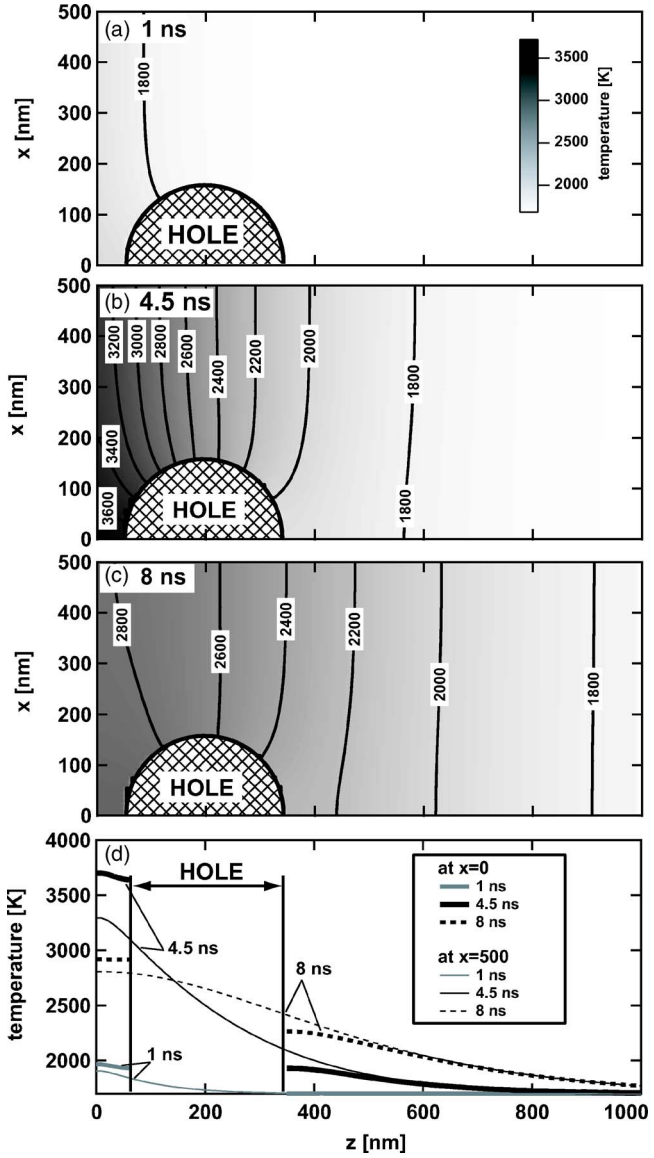

FIG. 8. (Color online) (a), (b), and (c) represent the temperature profiles in the x-z plane (y=0) at 1, 4.5, and 8 ns, respectively. (d) shows the depth dependence of the temperature (x=0 and 500 nm) at different times (R_h =150 nm, L_h=200 nm).

(i)] is ~400 K higher than that at the middle of the four holes [upper right in Fig. 7(a), position (ii)]. Figure 7(b) shows the temporal evolutions of the surface temperature at positions (i) and (ii). At position (ii), the maximum surface temperature is ~3300 K; therefore the surface cannot reach the melting point. On the other hand, the surface temperature at position (i) is higher than that at position (ii) and does reach the melting point. Because the heat cannot be conducted toward the z direction above the hole, the temperature increases locally due to the deposition of heat at the lid of the hole. Although the surface temperature may be overestimated because the surface reflectivity was assumed to be zero in the calculation, we can state that nonuniformity of the surface temperature arises due to the subsurface holes.

Figures 8(a)–8(c), show the temperature profiles in x-z plane at y=0 at the times of 1, 4.5, and 8 ns, respectively. Figure 8(d) shows the depth dependences of the temperature

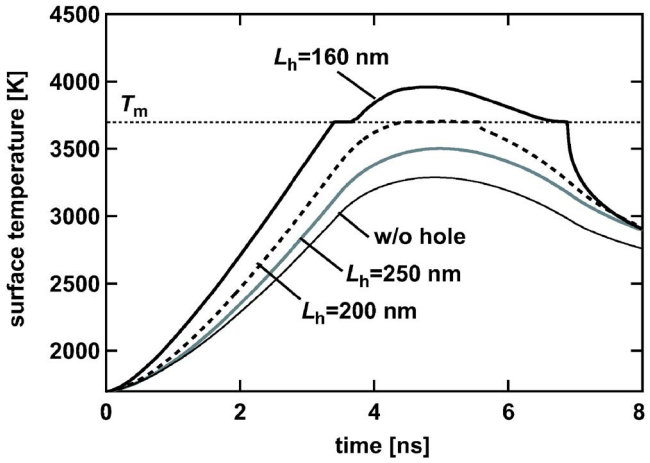

FIG. 9. (Color online) Temporal evolution of the surface temperature at position (i) for various L_h. (R_h=150 nm). The case without holes is also presented.

at x=0 and 500 nm at the times of 1, 4.5, and 8 ns. We can see that the characteristic length of heat transfer in tungsten during ~10 ns is less than 1 μm. Thus, the submicron size hole existing at $z<1$ μm has a great effect on the anomalous increase of the surface temperature. Although the temperature above the hole is almost uniform at 8 ns, a temperature gradient in the z direction exists during the time when a laser pulse is irradiated (at 1 and 4.5 ns). Therefore, the lid of the hole may not be totally melted, even if the surface above the hole reaches the melting point. To totally melt the lid of the hole, the thickness of the lid should be sufficiently thin, in this particular case typically several tens of nanometers. If the pulse duration is much longer than several nanoseconds, it is expected that the nonuniformity of the surface temperature becomes moderate because the deposition of heat is sufficiently mitigated and heat is conducted to a deeper region. Figure 9 shows the temporal evolution of the surface temperature at position (i) for various L_h. The maximum surface temperature around 4.5 ns increases as the distance between the hole and the surface decreases. The surface temperature reaches the melting point when the lid thickness, namely, the distance between the surface and the top of the hole, $L_h - R_h$, is less than ~50 nm.

The calculation results up to now have indicated that the surface temperature can reach the melting point when the thickness of a lid of a submicron hole is sufficiently thin. However, it is also shown that the surface temperature is considerably lower than the boiling point of 5900 K. Although the surface temperature may reach the boiling point if the thickness of the lid of the hole is several nanometers, it is not likely that the vaporization and ionization, which may lead to ablation of the material, are the main mechanisms that significantly enhance the roughness under the experimental conditions. We should note that it is not clear whether the melting itself would be the physical mechanism that significantly enhances the roughness, because some force is necessary to push out the tungsten melt from the surface to the plasmas.

We speculate that the temperature increase in the lid of the hole may lead to the explosion of the hole because the

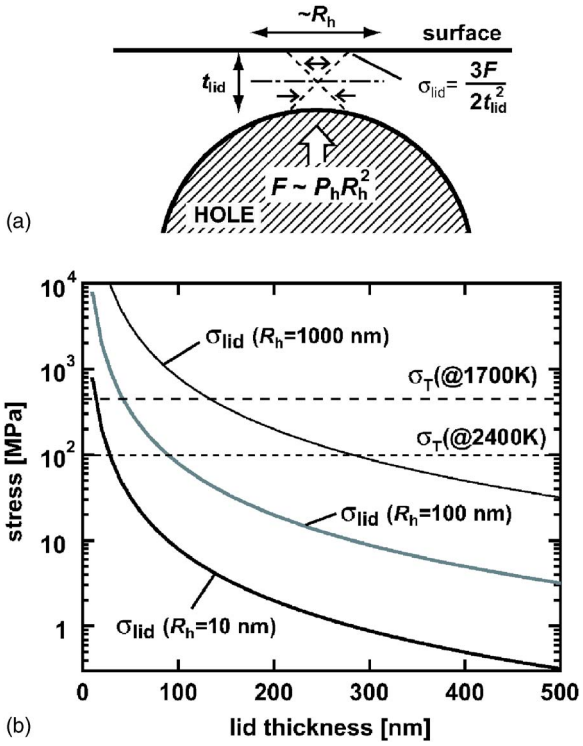

FIG. 10. (Color online) (a) Schematic illustration of a pressurized hole and the stress placed on the lid of the hole. (b) Ultimate tensile stress σ_T at 1700 and 2400 K, and the stress placed on the lid, σ_{lid}, as a function of the lid thickness.

pressure in the hole would be high enough. Assuming spherical equilibrium holes, the pressure in the hole P_h is maintained while satisfying the following relation,[30]

$$P_h = \frac{2\gamma}{R_h}, \tag{18}$$

where γ is the surface tension in N m^{-1}. Although the surface tension at a higher temperature is slightly greater than that at room temperature, the temperature dependence of γ is weak. Typically, the surface tension at room temperature is ~8% higher than that of the liquid metal.[30] Using a surface tension at room temperature of 2.65 N m^{-1},[30] the pressure in the helium hole is estimated to be ~35 MPa for R_h=150 nm. Since desorption from the inner surface of the hole is enhanced due to the transient temperature increase, the pressure in the hole may increase due to the transient temperature change. However, the effect on the pressure increase is negligible under the experimental conditions. From temperature desorption spectroscopy (TDS) experiments in Refs. 31 and 32, the change of the desorption rate of implanted helium is evaluated to be of the order of 10^{18}–10^{21} m^{-2} s^{-1}. Thus, the density increase due to desorption is $\lesssim 10^{21}\Delta t_{pulse} 4\pi R_h^2/(4\pi R_h^3/3)$ m^{-3}, which is much lower than the bulk helium density in a hole in which the pressure is greater than megapascals.

Figure 10(a) shows a schematic illustration of a pressurized hole and the stress placed on the lid, which can be evaluated in the same way as stress on a leaf spring.[33] Given that the hole's lid corresponds to a leaf spring with length, width and thickness of R_h, R_h, and t_{lid}, respectively, the maximum stress on the hole's lid, σ_{lid}, is obtained as

$$\sigma_{lid} \sim \frac{FR_h}{4}\frac{6}{R_h t_{lid}^2}, \tag{19}$$

where F is the force placed on the middle point of the lid. Using Eq. (18) and the relation $F \sim P_h R_h^2$, Eq. (19) becomes

$$\sigma_{lid} \sim \frac{3\gamma R_h}{t_{lid}^2}. \tag{20}$$

Therefore, the stress on the lid is estimated from the radius of the hole and the lid thickness. Figure 10(b) shows the calculated σ_{lid} as a function of lid thickness for R_h=10, 100, and 1000 nm. Because σ_{lid} is proportional to R_h and inversely proportional to t_{lid}^2, σ_{lid} increases with an increase of R_h and a decrease of t_{lid}. It is expected that the hole explodes if σ_{lid} exceeds the ultimate tensile stress σ_T, namely, when $\sigma_{lid} > \sigma_T$. The value of σ_T has strong temperature dependence, and it approximates to 0 as the temperature increases to the melting point. For example, $\sigma_T \sim 450$ MPa at 1700 K, whereas it decreases to ~100 MPa at 2400 K.[16] When the temperature of the lid reaches about 2400 K, the hole would explode if t_{lid} is sufficiently smaller than 100 nm, as shown in Fig. 10(b). Even when the temperature is lower than the melting point, an explosion can occur if $\sigma_{lid} > \sigma_T$.

Even in the case without a transient heat flux, holes may be broken if they bisect the surface in a manner similar to annealing helium implanted metals.[13] However, surface roughness cannot be significantly enhanced because the time scale of the process is very slow, typically $\gg$1 s.[14] On the other hand, explosions of the lids in response to laser pulses are accompanied by pressure releases from holes during the supershort time (10^{-8} s), so that a thin lid may be exploded into the vacuum.

From our experiments, roughness was enhanced only in cases where laser pulses were irradiated together with helium plasmas. Even if a substrate with helium holes was irradiated by the laser pulses, without simultaneous helium plasma irradiation, the surface was not further roughened. The results indicated that repetitive explosions of helium holes may lead to the enhancement of surface roughness. In other words, simultaneous irradiations of helium ion flux and laser pulses may have a drilling effect on tungsten and be accompanied by repetitive formations and explosions of subsurface holes. We would like to term this the "superdrilling effect." It is possible that local explosions of the surface occurred in response to every laser pulse, and finally after a surface has been irradiated by 18 000 pulses, the roughness of the surface is significantly enhanced, as shown in Fig. 4

Figure 11 shows the calculated maximum temperature at position (i) as a function of lid thickness, $L_h - R_h$, for various hole radii R_h. The surface temperature without holes was ~3250 K. Because the surface temperature above the hole is an indication whether an explosion of a hole occurs, we now discuss these dependences. The maximum surface temperature increases as decreasing $L_h - R_h$; furthermore, we can see that the temperature increase becomes greater as increasing R_h for the same $L_h - R_h$. From our experimental observations,

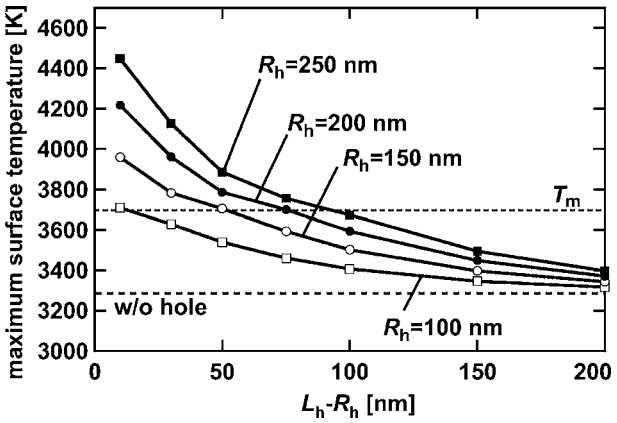

FIG. 11. Calculated maximum surface temperature above the hole [at position (i)] as a function of L_h-R_h for various hole radii R_h.

holes of several hundreds of nanometers in radius were observed, indicating that the lid of hole may melt if lid thickness is thin enough, typically <100 nm under the present conditions. Moreover, even if lid thickness is greater than 100 nm, σ_{lid} may exceed σ_T, and consequently, an explosion of a hole can occur.

For wide range of laser applications, optimal laser parameters for the treatment are discussed finally. In terms of pulse width, the effect may appear when the characteristic length of the heat transfer during the laser pulse width, $l_{\mathrm{heat}} \sim \sqrt{\kappa t_{\mathrm{pulse}}}$, is shorter than the penetration length of the surface modification ($\lesssim 1-2$ μm). From that perspective, the optimal pulse width corresponds to $\lesssim 10$ ns because thermal diffusivity κ is in the range from 2×10^{-4} (at $\sim$3000 K) to 4×10^{-4} m^2/s (at $\sim$1000 K). However, if $l_{\mathrm{heat}} \ll t_{\mathrm{lid}}$, the effect of hole does not appear because the heat does not reach the hole during the laser irradiation. Typically, the lid thickness is from several tens to several hundreds of nanometers, so that the effect of hole may not be significant if the pulse width is much less than a hundred picoseconds. Therefore, it can be said that optimal laser pulse width is typically $10^{-10} \lesssim t_{\mathrm{pulse}} \lesssim 10^{-8}$ s. In terms of the fluence, it is thought that the effect of the hole is not sufficient when the laser ablation occurs, since the phenomena may totally blow off the submicron structure such as the holes. Though the threshold fluence of ablation may change as varying the surface temperature, the effect of the blowoff may be significant when the laser fluence is greater than 5 J/cm^2 when the pulse width is about 5 ns.[34] Concerning the lower limit of the laser fluence, we can only say that the surface modification may not appear when the fluence is much lower than 0.1 J/cm^2 under the experimental condition in Fig. 4 because the lower limit may change as varying the surface temperature and surface conditions (lid thickness, hole size, etc.).

For future study, the physical mechanism is expected to be confirmed utilizing spectroscopic measurements of the W I line in response to laser pulses. Experimental investigations under different experimental conditions of the laser pulse energy, pulse width, surface temperature, helium ion flux, and so on will also be helpful to investigate the detailed characteristics of the superdrilling effect.

IV. CONCLUSION

Irradiation experiments of a nanosecond laser pulse to a tungsten substrate having submicron helium holes were performed in the divertor simulator NAGDIS-II. When laser pulses were irradiated to a tungsten surface that did not have subsurface holes, the surface became smoother due to the laser irradiation. On the other hand, when submicron helium holes existed near the surface, surface roughness was significantly enhanced when the sample was irradiated by laser pulses during the time that it exposed to helium plasmas. The penetration length of submicron holes became ~ 10 μm from $1-2$ μm. However, in deuterium plasmas and in vacuum, surface roughness was not enhanced by the laser pulse irradiations even if helium holes were formed under the experimental conditions. Therefore, simultaneous irradiations of helium ion and laser pulses are thought to be the crucial factors that enhance surface roughness.

To investigate the physical processes enhancing surface roughness, we analyzed surface temperature by solving a three-dimensional heat conduction equation with a model that included submicron holes near the surface. The calculation results show that the surface can reach the melting point locally if the distance between the holes and the surface was short enough. Typically, under the experimental conditions, lids of holes can melt if the thickness of hole's lid is sufficiently shorter than 100 nm. When lids of holes are heated around their melting point, the stress put on the lids due to the high pressure in the holes exceeds the ultimate tensile stress of tungsten, and consequently, an explosion of the hole can occur. It is speculated that enhancement of the surface roughness is caused by repetitive formation and explosions of subsurface holes. As a focus for future study, radiation from tungsten will be helpful to verify the proposed physical process, because the tungsten melt may be splashed and excited/ionized in plasmas if holes explode.

ACKNOWLEDGMENT

This work was supported in part by a Grant-in-Aid for Scientific Research from the Japan Society for the Promotion of Science (JSPS) Research Fellowships for Young Scientists (No. 17-7503).

[1] Y. Ueda, K. Tobita, and Y. Katoh, J. Nucl. Mater. **313–316**, 32 (2003).
[2] N. Yoshida, M. Miyamoto, K. Tokunaga, H. Iwakiri, H. Wakimoto, T. Fujiwara, and the TRIAM group, Nucl. Fusion **43**, 655 (2003).
[3] D. Nishijima, M. Y. Ye, N. Ohno, and S. Takamura, J. Nucl. Mater. **313–316**, 97 (2003).
[4] D. Nishijima, M. Ye, N. Ohno, and S. Takamura, J. Nucl. Mater. **329–333**, 1029 (2004).
[5] ITER Physics Basis Editors, ITER Physics Expert Group Chairs and Co-Chairs, ITER Joint Central Team, and Physics Integration Unit, Nucl. Fusion **39**, 2137 (1999).
[6] G. Federici, A. Loarte, and G. Strohmayer, Plasma Phys. Controlled Fusion **45**, 1523 (2003).
[7] S. Sharafat, N. M. Ghoniem, M. Anderson, B. Williams, J. Blanchard, L. Snead, and T. H. Team, J. Nucl. Mater. **347**, 217 (2005).
[8] S. Kajita, S. Kado, T. Shikama, B. Xiao, and S. Tanaka, Contrib. Plasma Phys. **44**, 607 (2004).
[9] S. Kajita, S. Kado, and S. Tanaka, Plasma Sources Sci. Technol. **14**, 566 (2005).
[10] S. Kajita, S. Kado, A. Okamoto, and S. Tanaka, Jpn. J. Appl. Phys., Part 1 **44**, 8661 (2005).

[11]S. Takamura, N. Ohno, D. Nishijima, and Y. Uesugi, Plasma Sources Sci. Technol. **11**, A42 (2002).
[12]S. Kajita, N. Ohno, S. Takamura, and T. Nakano, Phys. Plasmas **13**, 013301 (2006).
[13]R. E. Galindo, A. van Veen, J. H. Evans, H. Schut, and J. T. M. de Hosson, Nucl. Instrum. Methods Phys. Res. B **217**, 262 (2004).
[14]J. H. Evans, J. Nucl. Mater. **334**, 40 (2004).
[15]S. Kajita, D. Nishijima, N. Ohno, and S. Takamura, J. Plasma Fusion Res. **81**, 745 (2005).
[16]E. Koch-Bienemann, L. Berg, and G. Czack, *Gmelin Handbook of Inorganic Chemistry (Tungsten)* (Springer, Berlin, 1989), Suppl. A3.
[17]U. Seydel and W. Fucke, J. Phys. F: Met. Phys. **10**, L203 (1980).
[18]B. M. Smirnov, *Physics of Ionized Gases* (Wiley-Interscience, New York, 2001).
[19]P. Gustafson, Int. J. Thermophys. **6**, 395 (1985).
[20]Q. Qi, M. Wang, and G. Xu, Chem. Phys. Lett. **372**, 632 (2003).
[21]P. Ciarlet and J. Lions, *Handbook of Numerical Analysis* (North-Holland, Amsterdam, 1990), Vol. 1.
[22]J. Jim Douglas, Numer. Math. **4**, 41 (1962).
[23]J. R. Ho, C. P. Grigoropoulos, and J. A. C. Humphrey, J. Appl. Phys. **78**, 4696 (1995).
[24]*Thermophysical Property Handbook*, edited by the Japan Society of Thermophysical Properties (Yokendo, Tokyo 2000).
[25]T. Sugie, S. Kasai, M. Taniguchi, M. Nagatsu, and T. Nishitani, J. Nucl. Mater. **329–333**, 1481 (2004).
[26]M. Ye, S. Fukuta, N. Ohno, S. Takamura, K. Tokunaga, and N. Yoshida, J. Plasma Fusion Res. **3**, 265 (2000)..
[27]D. F. Price, R. M. More, R. S. Walling, G. Guethlein, R. L. Shepherd, R. E. Stewart, and W. E. White, Phys. Rev. Lett. **75**, 252 (1995).
[28]X. Y. Wang and M. C. Downer, Opt. Lett. **17**, 1450 (1992).
[29]J.-T. Lin and T. F. George, J. Appl. Phys. **54**, 382 (1983).
[30]S. Donnelly, Radiat. Eff. **90**, 1 (1985).
[31]K. Tokunaga *et al.*, J. Nucl. Mater. **313–316**, 92 (2003).
[32]Z. Fu, N. Yoshida, H. Iwakiri, and Z. Xu, J. Nucl. Mater. **329–323**, 692 (2004).
[33]M. F. Ashby and D. R. Jones, *Engineering Materials 1: An Introduction to Their Properties and Applications* (Pergamon, Oxford, 1980).
[34]Y. Kawakami and E. Ozawa, Appl. Surf. Sci. **218**, 175 (2003).